


Brainlike Networks of Nanowires and Nanoparticles: A Change of Perspective

Ryan. K. Daniels¹,¹ Matthew D. Arnold,² Zachary E. Heywood^{1,3},³ Joshua B. Mallinson,¹
Philip J. Bones^{1,3},³ and Simon A. Brown^{1,*}

¹*The MacDiarmid Institute for Advanced Materials and Nanotechnology, School of Physical and Chemical Sciences, Te Kura Matū, University of Canterbury, Private Bag 4800, Christchurch 8140, New Zealand*

²*School of Mathematical and Physical Sciences, University of Technology Sydney, PO Box 123, Broadway, NSW 2007, Australia*

³*Electrical and Computer Engineering, University of Canterbury, Private Bag 4800, Christchurch 8140, New Zealand*

 (Received 28 November 2022; revised 23 July 2023; accepted 21 August 2023; published 12 September 2023)

The connectivity of self-assembled networks of nanowires and nanoparticles is believed to strongly influence their performance in brainlike (neuromorphic) computing applications. Here we present a new perspective on the connectivity of these networks in which their neuronlike active elements are viewed in the same way as the nodes in artificial and biological neuronal networks. We consider two-dimensional and quasi-three-dimensional networks of nanowires and percolating networks of nanoparticles and show that, from this new perspective, they all have similar small-world characteristics. Other characteristics which may impact the computational performance of the networks are also investigated, including their assortativity and the scalefree nature of the nanoparticle networks. Taken together, these results allow comparison of key network characteristics for a variety of self-assembled nanoscale networks, and provide a basis for detailed investigations of computational performance.

DOI: [10.1103/PhysRevApplied.20.034021](https://doi.org/10.1103/PhysRevApplied.20.034021)

I. INTRODUCTION

Self-assembled networks of nanowires [1–13] and nanoparticles [14–24] have recently emerged as important candidate systems for brainlike (or neuromorphic) information processing. The essence of the approach is to take advantage of these networks' intrinsic dynamical properties to implement brain-inspired approaches to computation, such as reservoir computing [25,26]. Implementation of such approaches in hardware has the potential to overcome limitations in traditional integrated circuit technologies [27,28], while decreasing power consumption and improving performance [29,30].

It is well established that the intrinsic architectures of networks impact their dynamics, and in particular it has been shown that networks with scalefree and small-world properties provide important computational benefits [31–33]. There have therefore been significant efforts [9,12,18] to understand the connectivity of both networks of nanowires and nanoparticles (illustrated in the left column of Fig. 1). The basis of this approach is to construct connectivity maps in which the nanowires and nanoparticles are the nodes of the networks, and the connections between them are links (illustrated in Fig. 1, middle column, and discussed in detail below). This is a natural approach, and

is necessary, for example, for calculations of the electrical properties of the networks (through Kirchhoff's laws). However, in these static node maps (SNMs), the nodes are *passive, linear* elements (i.e., wires or particles) which do not modify signals that are transmitted through the network. This is very different from the situation in the biological brain and in artificial neural networks (ANNs) where the nodes are *dynamic, nonlinear* elements, that is, the nodes represent neurons which interact via (linear) synaptic connections.

This distinction is important because it has recently emerged that the memristive connections in self-assembled nanoscale networks exhibit dynamical, neuronlike behavior [7,11,20,34]. Hence, it is clear that a change of perspective is required in order to compare the network characteristics of self-assembled networks with those of neural networks: the neuronlike active elements of the networks (the memristive junctions) should be considered as the nodes, and the connections between them (provided by the wires or particles) should be the passive, linear links, just as in biological and ANNs. This perspective is essential to the design of physical computing systems based on self-organized networks which aim to emulate the structure and associated functionality of neural networks. Here we present a detailed analysis of both nanowire networks (NWNs) and percolating networks of nanoparticles (PNNs) from this new perspective. As the cornerstone of

*simon.brown@canterbury.ac.nz

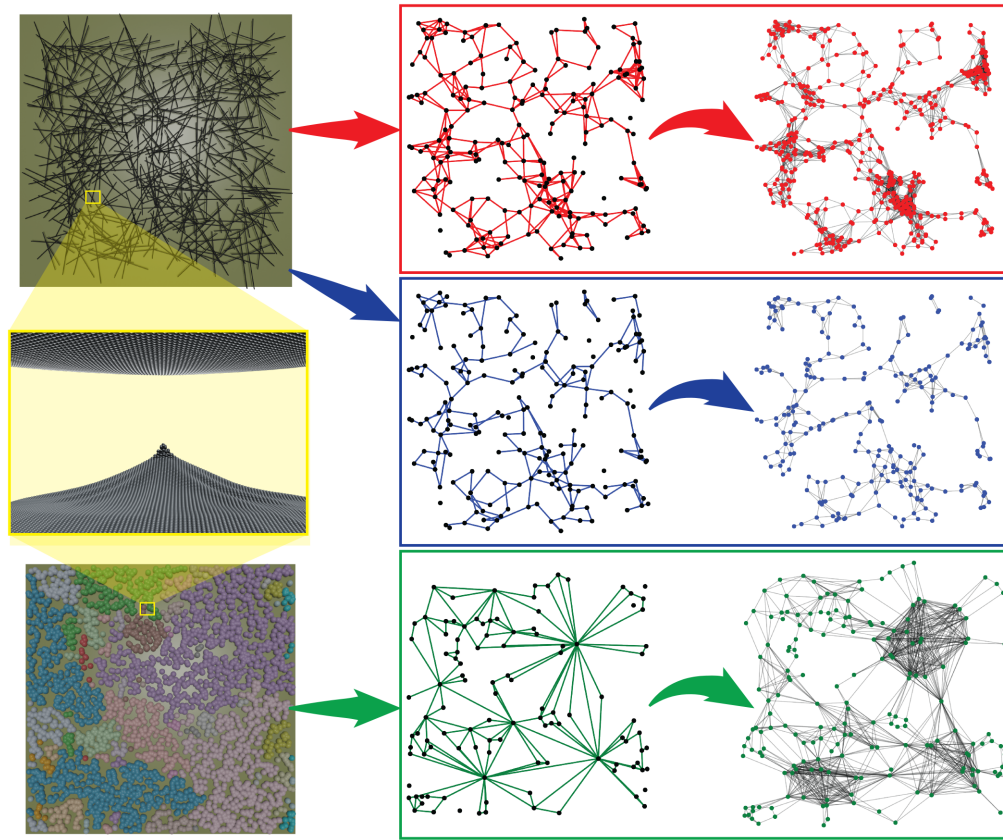


FIG. 1. Process for construction of dynamic node maps (DNMs). The left column shows examples of a nanowire network (NWN; top) and a percolating network of nanoparticles (PNN; bottom), and the electric-field-driven formation of a “hillock” of atoms in the tunnel gaps between the wires or nanoparticles (center). These hillocks are precursors to the formation of filaments that bridge the gaps and exhibit memristive properties (see main text). The middle column shows static node maps (SNMs) in which the wires and groups of nanoparticles are the nodes in the network. For the NWNs [two-dimensional (2D; top row) and quasi-three-dimensional (Q3D; middle row)], the nodes are the midpoints of the nanowires, and the links represent the memristive junctions formed between the wires. There are fewer connections in the 3D case because of stacking effects [12]. In the PNN (bottom), nanoparticles coalesce to form groups (each colored differently in the bottom left panel). The nodes are then the group centroids, and the links are gaps formed between groups (these are also the memristive junctions). The right column shows the DNMs, in which the memristive junctions are the nodes of the networks and the links represent connections via wires/groups.

this change in approach, which is explained in detail below, we introduce the concept of *dynamic* node maps (DNMs) for these networks. We present a detailed characterization of their properties and show that despite significant differences in the SNMs for NWNs as compared to PNNs, the DNMs are surprisingly similar to each other. We show that, in fact, the DNMs of *all* investigated networks exhibit small-world properties, that is, they are highly clustered and have small path lengths between nodes [35], and all DNMs are assortative.

II. NETWORK MODELS

Both NWNs and PNNs (Fig. 1, left column) are created using simple deposition processes [1–24]. The building blocks (nanowires, particles) are deposited randomly on insulating substrates and electrodes are provided to allow

input signals to be injected into the networks, and outputs to be read, as required for computation. There are, however, key differences. Nanowires are typically surrounded by an insulating shell, so that when they land on previously deposited wires a memristive tunnel gap (Fig. 1, center panel of left column; see discussion in next section) is created at each point of contact between wires [1–3,5]. The wires form quasi-three-dimensional (Q3D) stacks [12], but since the wires are often assumed to form perfectly planar, two dimensional (2D) networks, we consider both Q3D and 2D cases here. Nanowire deposition is simulated by randomly choosing the placement and orientation of the wires within a square deposition area. Where two wires intersect, a connection (memristive junction) is formed and the connectivity is stored in an adjacency matrix. Wires in the 2D networks are considered to be 1D lines, and therefore lie in a 2D plane and are allowed to interpenetrate.

Wires in the Q3D networks are considered to be 3D cylinders which stack vertically. Deposition occurs sequentially, with previous wires affecting the position of a new wire in 3D space. The plane has dimensions $30\ \mu\text{m}$ and the wires are $6\ \mu\text{m}$ long, which means that the percolation threshold is at $N \sim 140$ wires. For more details, see [12].

Metallic nanoparticles, on the other hand, have no protective shell and coalesce when they land on each other, forming extended, well-connected *groups* (Fig. 1, bottom left); the deposition is terminated at the percolation threshold (onset of conduction) [14–16,21], ensuring that the groups of particles are separated from one another by memristive tunnel gaps. The nanoparticles are simulated as uniform disks deposited randomly within a square deposition area, and are allowed to overlap with each other. This overlapping simulates the coalescence between neighboring particles, leading to the formation of groups of well-connected particles. When the surface coverage is below a critical threshold, no single group spans the entire deposition area. The conduction of the network is therefore due to the tunnel currents that flow across small gaps between groups. The centroids of the groups are taken to be the nodes, and the connections between groups, defined as the minimum distance between neighboring group boundaries, are stored in an adjacency matrix (as with the NWNs). For more details, see [12,18,19,36].

We emphasize that after deposition the overall structure of both the NWNs and PNNs is fixed, and the dynamical (memristive) behavior takes place only in the tunnel gaps, where atomic or nanoscale filaments are formed. This is in contrast to other types of device in which memristive behavior results from significant rearrangements of nanoparticles [37].

Both NWNs and PNNs can be considered within the framework of percolation theory, but experimental considerations mean that the two types of network are constrained in different ways. NWNs can be fabricated with a range of wire densities *above* the percolation threshold [10], and so it is important to investigate the properties of networks as a function of the number of wires deposited (N), at a fixed system size. In contrast, PNNs are always prepared *at* the percolation threshold, and scaling laws [38,39] suggest that network properties will change as a function of system size (we consider square systems of size $W \times W$ particle diameters). We therefore investigate the connectivity of NWNs and PNNs as a function of these different natural variables (N and W , respectively), before comparing results and drawing conclusions.

III. DYNAMICAL, NEURONLIKE BEHAVIOR IN TUNNEL GAPS

The basic nonlinear units facilitating computation in the networks are the tunnel gaps. The tunnel gaps that form between neighboring nanoparticle groups and between

touching nanowires act as switching sites: upon application of an external voltage stimulus, atomic-scale filaments can be formed (and subsequently broken) in the tunnel gaps [14], resulting in changes in the gap conductance and consequently in the network conductance (G). These tunnel gaps, regardless of the type of system, are memristive: their resistance responds nonlinearly to changes in applied voltage and exhibits memory of previous stimuli [40].

The atomic-scale behavior is illustrated in Fig. 1 (center panel of left column): when a bias voltage is applied across the gap, it causes the migration of ions and, depending on the system, an atomic or nanoscale filament begins to form [41–43]. In the low-bias regime, the conductance is low because the current flow across the gap is via quantum tunneling. As the filament grows (shrinks), the width of the tunneling barrier decreases (increases), causing a non-linear change in conductance for each junction. At higher bias, the filament can bridge the gap, causing a transition to a high-conductance Ohmic state.

Importantly, the effect of the applied electric field/current is cumulative, that is, both formation and destruction of the atomic-scale filaments can be viewed as integrating the applied signals until filament formation/destruction (“firing”). These processes are therefore qualitatively similar to integration and fire mechanisms in biological neurons [44,45]. A variety of neuronlike behaviors have been described in different networks and individual devices, relying on both atomic-scale and nanoscale mechanisms: the literature includes several studies that demonstrate brainlike properties such as neural avalanching and that compare experiments with simulations [7,19] as well as recent reviews [10]. Note, however, that since the focus of the present work is on the characteristics of the *networks* of memristive elements, neither the type of memristor under consideration nor the way that they are modeled affects the analysis presented below. It should also be emphasized that we are focused here on basic network characteristics (in the absence of stimuli) because the architecture of the network affects its dynamical properties, and hence its possible computational applications [7,17,19,46].

IV. A CHANGE OF PERSPECTIVE

Figure 1 demonstrates the construction of DNMs for all three types of networks [2D NWNs (top row, red), Q3D NWNs (center row, blue) and PNNs (bottom row, green)]. The left column in Fig. 1 shows the physical network structure; the top views of the 2D and 3D NWNs are the same, as they differ only in their connectivity. The center column captures the connectivity of the networks in the corresponding SNMs: each wire or group of particles is a node in the network (black circles) and the links between them (colored lines) represent memristive tunnel gaps that connect the nodes. The right column in Fig. 1 shows the transformation to the DNM, in which each neuronlike

tunnel gap is represented as a colored node and the black lines represent passive links between them. The DNM is constructed simply by determining which *links* are connected via *nodes* in the corresponding SNM. This process is similar to the construction of so-called line graphs in graph theory [47]. The resultant DNM visualizes the connectivity between the active elements (“neurons” [7,20]) and captures the topology of the ANN contained within the NWN or PNN.

In the following we compare the detailed properties of the DNMs and SNMs for all three network types.

V. RESULTS AND DISCUSSION

A. Basic connectivity analysis

We start by considering the degree of each node in the network maps and the lengths L of the paths between nodes. The degree, k , of a node is the number of links

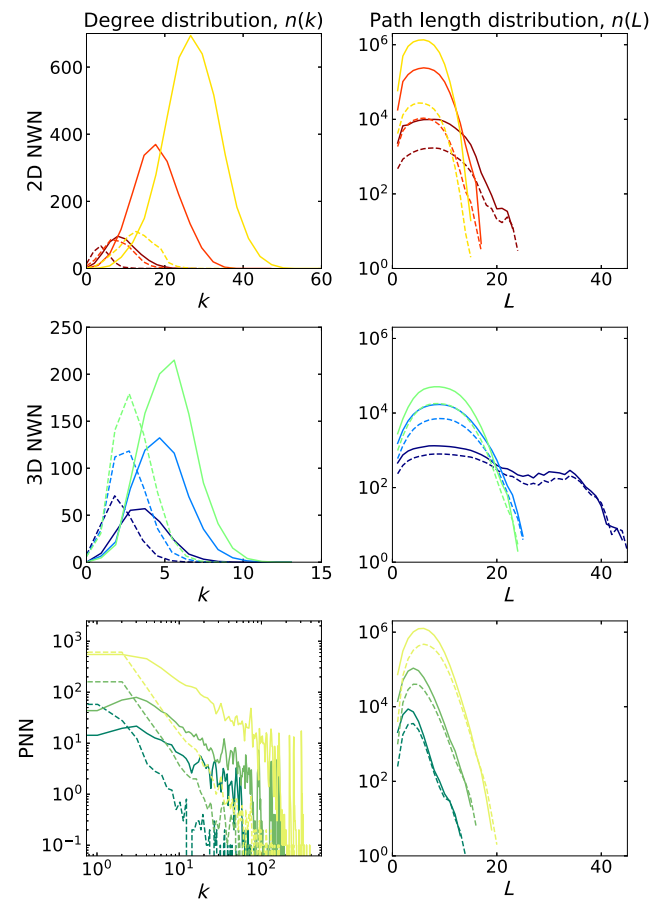


FIG. 2. Key characteristics of the networks. Left column: degree distributions $n(k)$. Right column: path length distributions $n(L)$. 2D NWNs (top row, red), Q3D NWNs (middle row, blue) and PNNs (bottom row, green). SNMs, dashed lines; DNMs, solid lines. For the NWNs data are shown for $N = 200, 400$, and 600 wires, and for the PNNs $W = 50, 100, 200$; the progression from dark to light colors indicates increasing N, W .

that connect that node to other nodes. Figure 2 shows the degree distributions $[n(k), \text{left}]$, for $N = 200, 400, 600$ (for the NWNs) and $W = 50, 100, 200$ (for the PNNs). The data for SNMs (DNMs) are shown with dashed (solid) lines. The degree distributions for NWNs are approximately normal, both for the SNMs and DNMs, but the distributions are broader for the 2D case (note the different horizontal scales in these two panels) because the wires all lie in a 2D plane, and therefore intersect all other wires deposited before or after them. In both 2D and Q3D networks, the DNMs have much larger mean degrees [$\bar{k} = (1/N) \sum_i^N k_i$; see Fig. 3, left column], although this difference is more striking in the 2D networks. In contrast the degree distributions for the PNNs are power laws [18], with a shallower slope for the DNMs (note the logarithmic scales). The essential origin of these changes is that when the transformation to the DNMs occurs, there are many more nodes and connections between nodes than in the original SNMs (see Appendix for an illustrative example and detailed discussion).

The path length between nodes i and j , L_{ij} , is the shortest sequence of links that connects them [35]. Figure 2 (right column) shows the path length distributions $n(L)$ for all networks. While there are some differences in detail, such as the increase in the width of the distributions for the Q3D NWNs compared to the 2D NWNs (the path between any pair of wires/junctions can be a complex route through the 3D stack, and paths can be circuitous, especially for small N), in each case the path length distributions for the static and DNMs are remarkably similar to one another. This is simply because the number of nodes and links are directly related to each other: as the number of nodes increases in the SNMs, so too does the number of links (compare center and right columns in Fig. 3).

B. Small-world nature of the networks

Small-world networks are highly clustered and have small path lengths between nodes [35]. It has previously been demonstrated that various biological and physical networks are small-world including *Caenorhabditis elegans* neural networks and macaque monkey brain regions [48,49], and 2D NWNs [12,50].

Figure 4 shows a comparison of the mean path lengths \bar{L} (left column), mean local clustering \bar{C} (middle column), and small-world propensity (right column) for the SNMs (dashed lines) and DNMs (solid lines). Again each row corresponds to a different network type: 2D NWNs (top row, red), Q3D NWNs (middle row, blue), and PNNs (bottom row, green). All displayed quantities are the mean values obtained from 10 network realizations, with uncertainties representing standard deviations. \bar{L} (i.e., $[1/N(N-1)] \sum_{i \neq j}^N L_{ij}$) increases at a slower rate for the Q3D networks than for the 2D networks. This is

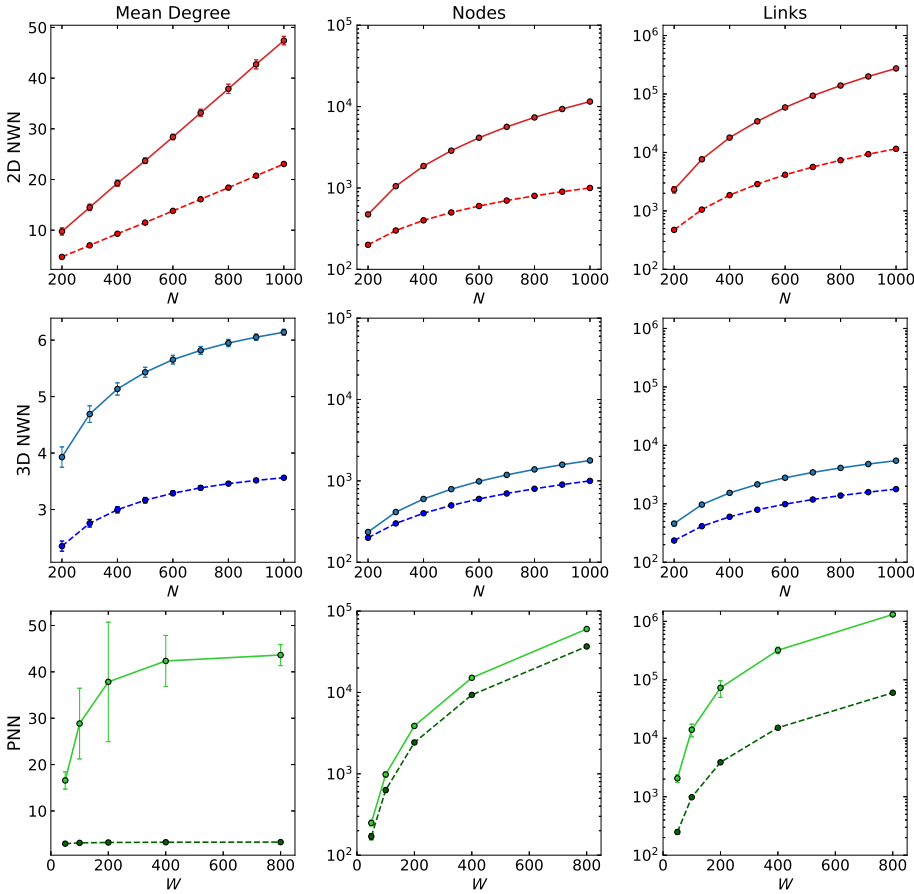


FIG. 3. Dependence of mean degree \bar{k} (left column), the mean number of nodes (center), and the mean number of links between nodes (right) on the number of nanowires, N (for the NWNs), and the system size, W (for the PNNs). 2D NWNs (top row, red), Q3D NWNs (middle row, blue) and PNNs (bottom row, green). SNMs, dashed lines; DNMs, solid lines. For the NWNs the transformation from the SNM to the DNM causes relatively modest changes in all three quantities. In contrast, the transformation causes a dramatic increase in \bar{k} for the PNNs, since the fractal groups of nanoparticles connect many tunnel gaps (see Fig. 1 in the main text.).

because wires at the top of the stack in the Q3D networks cannot connect with wires at the bottom [12]. For all networks, \bar{L} values for the DNMs are very similar to those for the SNMs, reflecting the similarities in the path length distributions shown in Fig. 2.

The second column in Fig. 4 shows \bar{C} for the different networks. For any node i with degree k_i , the local clustering coefficient [35] is given by

$$C_i = \frac{1}{k_i(k_i - 1)} \sum_{j,k} A_{ij} A_{ik} A_{jk}, \quad (1)$$

where A_{ij}, A_{ik}, A_{jk} are elements of the adjacency matrix. The mean local clustering coefficient is then $\bar{C} = (1/N) \sum_{i=1}^N C_i$. The SNMs for the 2D NWNs and the PNNs have a high degree of clustering, whereas those for the Q3D NWNs have low clustering, similar to random networks. However, after the transformation is made to the DNMs, clustering increases for all network types. The most dramatic increase is for the Q3D NWNs where the increase in \bar{C} causes a significant increase in the small-world propensity ϕ (Fig. 4, right column, middle row). ϕ quantifies the small-world nature of the networks by mapping them onto corresponding regular and random Watts-Strogatz networks with the same number of nodes

and degree distribution [48]:

$$\phi = 1 - \sqrt{\frac{\Delta_C^2 + \Delta_L^2}{2}}, \quad (2)$$

where the deviation of network clustering from those of a regular lattice is

$$\Delta_C = \frac{C_{\text{latt}} - \bar{C}}{C_{\text{latt}} - C_{\text{rand}}} \quad (3)$$

and the deviation of network path lengths from those of a random network is

$$\Delta_L = \frac{L_{\text{obs}} - L_{\text{rand}}}{L_{\text{latt}} - C_{\text{rand}}}. \quad (4)$$

Values of $\phi > 0.6$ signify small-world properties [48], and so *the DNMs are small-world for all network types*. This is a dramatic change for the Q3D NWNs, as the SNMs are *not* small-world. Remarkably, there is no significant change in small-world character for the other network types, despite significant changes in the maps shown in Fig. 1, and in the degree distributions (Fig. 2).

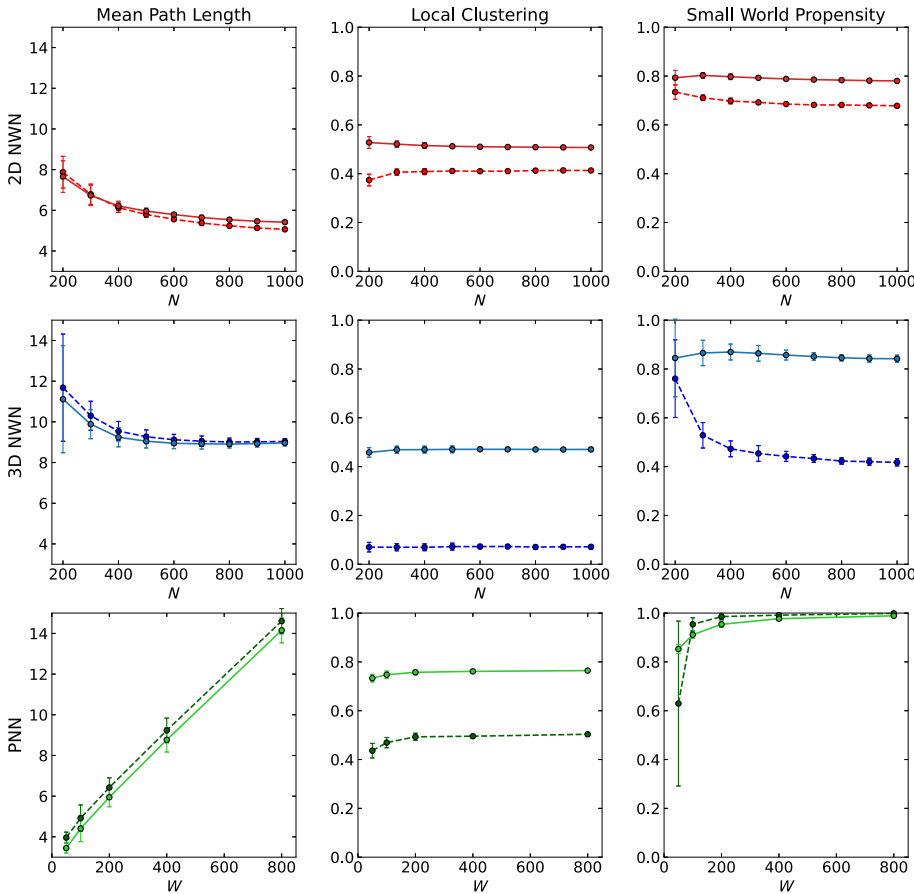


FIG. 4. Small-world nature of the networks. Dependence of mean path length (left), mean local clustering coefficient (middle), and small-world propensity (right) on the number of nanowires (N , for the NWNs) or the system size (W , for the PNNs). 2D NWNs (top row, red), Q3D NWNs (middle row, blue) and PNNs (bottom row, green). SNMs, dashed lines; DNMs, solid lines.

C. Discussion of other network characteristics

The results presented in the previous sections establish a clear basis for comparison of the different networks of interest, using multiple different metrics. Since the transformation of the SNMs to DNMs results in rather similar small-world characteristics for all networks we now consider some additional network properties that have previously been shown to be biologically relevant and to impact on computational performance in neural networks.

We begin by considering the *global* clustering for each network [Fig. 5 (left column)], since it is correlated with the assortativity [51,52] that will be discussed next. The global clustering coefficient [53], C_{global} , is the ratio of closed triplets to all triplets:

$$C_{\text{global}} = \frac{\text{closed triplets}}{\text{open} + \text{closed triplets}}, \quad (5)$$

where an open triplet is defined as three nodes connected by two links, and a closed triplet is defined as three nodes connected by three links. In most cases, the global clustering coefficients are similar to the local clustering coefficients. The exception is for the PNNs where the transformation from the SNM to the DNM causes a dramatic change: the global clustering coefficients for the SNMs (DNMs) are significantly lower (higher) than the local

clustering coefficients shown in Fig. 4. This is because the calculation of the global clustering places greater (lesser) weight on high-degree (low-degree) nodes compared to the local clustering.

Assortativity is a measure of the correlation between nodes based upon some property [54]. For example, in social networks, a person is more likely to be connected to people of a similar age than to people with radically different ages. The degree assortativity [54] is the Pearson correlation coefficient of the degree between pairs of connected nodes, given by

$$r = \frac{\sum_{ij} ij (e_{ij} - a_i b_j)}{\sigma_a \sigma_b}, \quad (6)$$

where e_{ij} is the fraction of links that connect nodes of degree i to nodes of degree j , and in undirected networks is symmetric. a_i and b_j are the fraction of links that start and finish at nodes with degrees i and j respectively (note that for undirected graphs, $a_i = b_j$). σ_a and σ_b are the standard deviations of the distributions a and b . Values of r vary between -1 and 1 .

Here we examine assortativity based on the degree of each node. High assortativity indicates that high-degree (low-degree) nodes are often connected to other

high-degree (low-degree) nodes, whereas negative assortativity (also called disassortativity) indicates that high-degree nodes are often connected to low-degree nodes. Many biological networks are disassortative, contrasting with social networks which have high assortativity. Figure 5 (right column) shows the assortativity for each network. The SNMs for the Q3D NWNs are disassortative, and the corresponding DNMs are assortative, and a similar but more modest change is observed for the 2D NWNs (SNMs are assortative, and DNMs are highly assortative). This increase in assortativity is driven by the increase in global clustering since there is a clear correlation between high assortativity and networks with a transitive bias [51,52]: when the global clustering is high (low), the assortativity is also high (low).

The change in assortativity for the PNNs is more dramatic. The SNMs for PNNs have the lowest (most negative) values of the assortativity among all networks

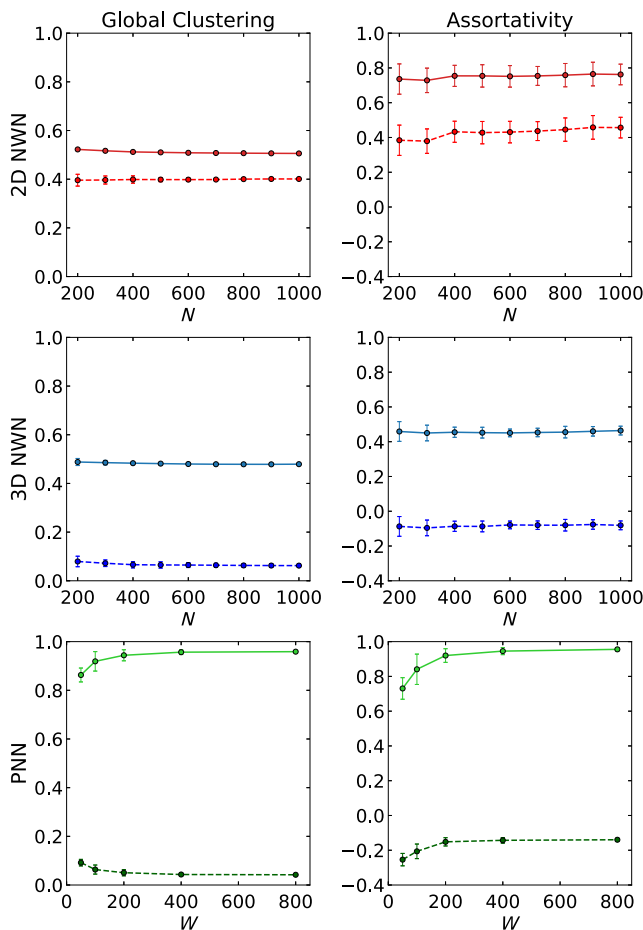


FIG. 5. Assortativity for the various networks. Dependence of the global clustering (left column) and assortativity (right column) on the number of nanowires (N , for the NWNs) or the system size (W , for the PNNs). 2D NWNs (top row, red), Q3D NWNs (middle row, blue) and PNNs (bottom row, green). SNMs, dashed lines; DNMs, solid lines.

considered here, whereas the corresponding DNMs are the most assortative. The wheel-and-spoke-type pattern observed in the SNM (Fig. 1, center panel of bottom row) is a common feature of disassortative networks with power-law degree distributions such as in *C. elegans* neural and protein connectivity maps [52,55]. The high-degree nodes act as hubs that connect mainly to smaller nodes with low degree. This connectivity is destroyed in the transformation to the DNMs as the global clustering and therefore the assortativity increases dramatically, that is, many tunnel gaps (nodes in the DNMs) have high k (see Fig. 4) and are connected to other tunnel gaps with high k via conducting groups of nanoparticles.

Assortativity has been shown to significantly impact computational performance [56], and it can influence the order of phase transitions and lead to explosive synchronization in oscillator networks [57]. Furthermore, it has been shown that robustness to noise is greatly enhanced in assortative neural networks, especially if it is the hub neurons that store the information, while disassortative networks are less resilient [58,59]. This is highly relevant to the present work, because the DNM perspective establishes the neuronlike memristive connections as the network node, and, at least for the PNNs, the effect of transforming the SNM to the DNM is dramatic. The present results are promising, but it must be acknowledged that in each case the existing literature [56–59] focuses on specific types of neural or oscillator networks, and so it remains to be demonstrated whether the computational performance of the NWNs and PNNs will indeed be impacted by the particular network properties (scalefree, small-world, local and global clustering, and assortativity) studied here.

VI. CONCLUSION

In conclusion, we have presented a new perspective on the connectivity of nanowire and nanoparticle networks which leads to clear differences in topological properties (in comparison to previously published analyses), such as higher mean degrees and higher local clustering coefficients for all network types considered. We emphasize that while small-world properties of PNNs and NWNs have been identified previously [12,50], neither the need to consider DNMs, nor the properties of the DNMs have been considered previously. The key structural differences that underpin the differences in properties of the PNNs and NWNs are: (i) that in PNNs the nanoparticles overlap with each other to form groups of well-connected particles that are separated by tunnel gaps that have a range of sizes [19,51], whereas nanowires are usually coated with materials that form relatively uniform memristive gaps between the wires [4]; and (ii) the nanoparticles are deposited to the percolation threshold (so that the networks are poised at the threshold for conduction) whereas the NWNs are usually well above the percolation threshold.

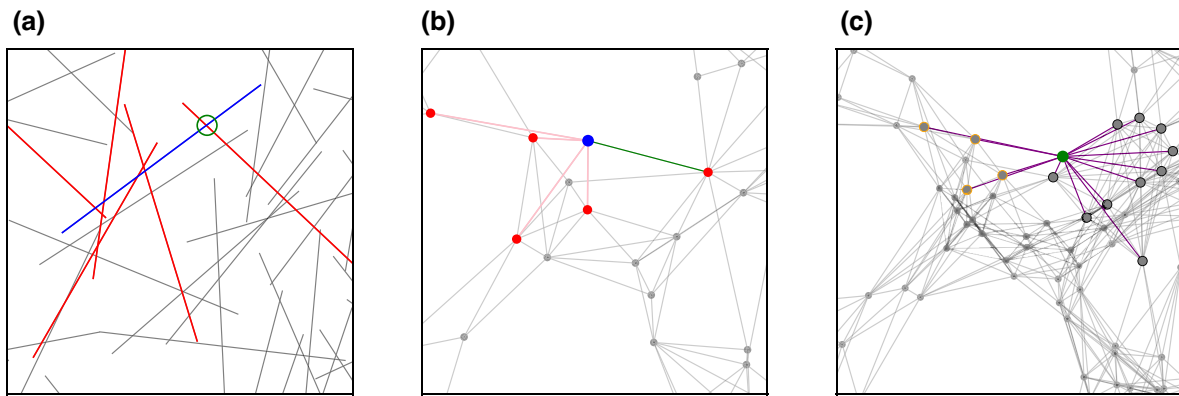


FIG. 6. (a) Portion of a NWN, highlighting a single wire (blue) and the wires it is connected to (red). (b) Static node map corresponding to (a). (c) DNM corresponding to (b).

The change of perspective presented here means that the neuronlike active elements in self-assembled nanoscale networks are viewed as equivalent to the nodes in artificial and biological neuronal networks. This change of perspective is required in order to allow direct comparison of properties of the networks (degree distributions, small-world characteristics, assortativity) but we emphasize that the electrical characteristics of the NWNs and PNNs are unaffected: the application of Kirchhoff's laws requires the network to be considered from the point of view of the original SNMs. When considered as DNMs, 2D NWNs, Q3D NWNs and PNNs all have small-world characteristics and high assortativity, suggesting that the performance of neuromorphic devices based on these networks might be similar. The main differences in the DNMs are that PNNs additionally have a scalefree network architecture similar to that of the biological brain [18]. This scale-free architecture, which is maintained in the transformation from SNMs to DNMs, is important for computational performance [46].

ACKNOWLEDGMENTS

The authors gratefully acknowledge financial support from the MacDiarmid Institute for Advanced Materials and Nanotechnology and the Marsden Fund, New Zealand.

APPENDIX: ILLUSTRATION OF THE EFFECT OF THE TRANSFORMATION ON THE MEAN DEGREE.

The effect of the transformation from an SNM to a DNM on the mean degree is described in this appendix. Since the mean degree in the SNM is $\langle k \rangle$, which is greater than 1, the transformation to the DNM generates $\langle k \rangle$ times more nodes in the DNM. The number of links in the DNM is also significantly higher. This can be visualized for the specific example illustrated in Fig. 6. The blue wire in (a) makes connections to five red wires (i.e., there are five

memristive gaps), and so the degree of the blue node in the SNM shown in (b) is 5. Now consider the memristive gap highlighted by the green circle in (a) and represented by the green link in (b). This memristive gap is a node in the DNM [green node in (c)] and is connected to four other nodes (highlighted by the gold circles) *plus* the gaps between the far right red wire and any gray wire that crosses it (there are 10, highlighted by the black circles). Hence the degree of the green node in the DNM is significantly higher than that of the original blue wire in the SNM. The same is true for *every* memristive gap. The average degree of each node in the DNM is therefore higher than those in the SNM. And since the number of nodes in the DNM is already greater than that in the SNM, both N and $\langle k \rangle$ increase as a result of the transformation. These changes underpin the changes in other properties of the network that are discussed in the other figures.

- [1] A. Z. Stieg, A. V. Avizienis, H. O. Sillin, C. Martin-Olmos, M. Aono, and J. K. Gimzewski, Emergent criticality in complex Turing B-Type atomic switch networks, *Adv. Mater.* **24**, 286 (2012).
- [2] H. G. Manning, F. Niosi, C. G. da Rocha, A. T. Bellew, C. O'Callaghan, S. Biswas, P. F. Flowers, B. J. Wiley, J. D. Holmes, and M. S. Ferreira, *et al.*, Emergence of winner-takes-all connectivity paths in random nanowire networks, *Nat. Commun.* **9**, 3219 (2018).
- [3] H. Tanaka, M. Akai-Kasaya, A. TermehYousefi, L. Hong, L. Fu, H. Tamukoh, D. Tanaka, T. Asai, and T. Ogawa, A molecular neuromorphic network device consisting of single-walled carbon nanotubes complexed with polyoxometalate, *Nat. Commun.* **9**, 2693 (2018).
- [4] A. Diaz-Alvarez, R. Higuchi, P. Sanz-Leon, I. Marcus, Y. Shingaya, A. Z. Stieg, J. K. Gimzewski, Z. Kuncic, and T. Nakayama, Emergent dynamics of neuromorphic nanowire networks, *Sci. Rep.* **9**, 14920 (2019).
- [5] G. Milano, G. Pedretti, M. Fretto, L. Boarino, F. Benfenati, D. Ielmini, I. Valov, and C. Ricciardi, Brain-inspired

- structural plasticity through reweighting and rewiring in multi-terminal self-organizing memristive nanowire networks, *Adv. Intell. Syst.* **2**, 2000096 (2020).
- [6] Q. Li, A. Diaz-Alvarez, D. Tang, R. Higuchi, Y. Shingaya, and T. Nakayama, Sleep-dependent memory consolidation in a neuromorphic nanowire network, *ACS Appl. Mater. Interfaces* **12**, 50573 (2020).
- [7] J. Hochstetter, R. Zhu, A. Loeffler, A. Diaz-Alvarez, T. Nakayama, and Z. Kuncic, Avalanches and edge-of-chaos learning in neuromorphic nanowire networks, *Nat. Commun.* **12**, 4008 (2021).
- [8] C. S. Dunham, S. Lilak, J. Hochstetter, A. Loeffler, R. Zhu, C. Chase, A. Z. Stieg, Z. Kuncic, and J. K. Gimzewski, Nanoscale neuromorphic networks and criticality: A perspective, *J. Phys.: Complex.* **2**, 042001 (2021).
- [9] A. Loeffler, R. Zhu, J. Hochstetter, A. Diaz-Alvarez, T. Nakayama, J. M. Shine, and Z. Kuncic, Modularity and multitasking in neuro-memristive reservoir networks, *Neuromorphic Comput. Eng.* **1**, 014003 (2021).
- [10] Z. Kuncic and T. Nakayama, Neuromorphic nanowire networks: Principles, progress and future prospects for neuro-inspired information processing, *Adv. Phys. X* **6**, 1894234 (2021).
- [11] G. Milano, G. Pedretti, K. Montano, S. Ricci, S. Hashemkhani, L. Boarino, D. Ielmini, and C. Ricciardi, In materia reservoir computing with a fully memristive architecture based on self-organizing nanowire networks, *Nat. Mater.* **21**, 195 (2021).
- [12] R. K. Daniels and S. A. Brown, Nanowire networks: How does small-world character evolve with dimensionality?, *Nanoscale Horiz.* **6**, 482 (2021).
- [13] R. K. Daniels, J. B. Mallinson, Z. E. Heywood, P. J. Bones, M. D. Arnold, and S. A. Brown, Reservoir computing with 3D nanowire networks, *Neural. Netw.* **154**, 122 (2022).
- [14] A. Sattar, S. Fostner, and S. A. Brown, Quantized Conductance and Switching in Percolating Nanoparticle Films, *Phys. Rev. Lett.* **111**, 136808 (2013).
- [15] S. K. Bose, J. B. Mallinson, R. M. Gazoni, and S. A. Brown, Stable self-assembled atomic-switch networks for neuromorphic applications, *IEEE Trans. Electron Devices* **64**, 5194 (2017).
- [16] S. K. Bose, S. Shirai, J. B. Mallinson, and S. A. Brown, Synaptic dynamics in complex self-assembled nanoparticle networks, *Faraday Discuss.* **213**, 471 (2019).
- [17] J. B. Mallinson, S. Shirai, S. K. Acharya, S. K. Bose, E. Galli, and S. A. Brown, Avalanches and criticality in self-organized nanoscale networks, *Sci. Adv.* **5**, eaaw8438 (2019).
- [18] S. Shirai, S. K. Acharya, S. K. Bose, J. B. Mallinson, E. Galli, M. D. Pike, M. D. Arnold, and S. A. Brown, Long-range temporal correlations in scale-free neuromorphic networks, *Netw. Neurosci.* **4**, 432 (2020).
- [19] M. Pike, S. K. Bose, J. B. Mallinson, S. Acharya, S. Shirai, E. Galli, S. Weddell, P. Bones, and A. M. S. A. Brown, Atomic scale dynamics drive brain-like avalanches in percolating nanostructured networks, *Nano Lett.* **20**, 3935 (2020).
- [20] S. Acharya, E. Galli, J. B. Mallinson, S. K. Bose, F. Wagner, Z. Heywood, P. Bones, and A. M. S. A. Brown, Stochastic spiking behaviour in neuromorphic devices enables true random number generation, *ACS Appl. Mater. Interfaces* **13**, 52861 (2021).
- [21] C. Minnai, A. Bellacicca, S. A. Brown, and P. Milani, Facile fabrication of complex networks of memristive devices, *Sci. Rep.* **7**, 7955 (2017).
- [22] M. Mirigliano, F. Borghi, A. Podestà, A. Antidormi, L. Colombo, and P. Milani, Non-ohmic behavior and resistive switching of Au cluster-assembled films beyond the percolation threshold, *Nanoscale Adv.* **1**, 3119 (2019).
- [23] M. Mirigliano, D. Decastri, A. Pullia, D. Dellasega, A. Casu, A. Falqui, and P. Milani, Complex electrical spiking activity in resistive switching nanostructured Au two-terminal devices, *Nanotechnology* **31**, 234001 (2020).
- [24] N. Carstens, B. Adejube, T. Strunskus, F. Faupel, S. Brown, and A. Vahl, Brain-like critical dynamics and long-range temporal correlations in percolating networks of silver nanoparticles and functionality preservation after integration of insulating matrix, *Nanoscale Adv.* **4**, 3149 (2022).
- [25] M. Lukoševičius and H. Jaeger, Reservoir computing approaches to recurrent neural network training, *Comput. Sci. Rev.* **3**, 127 (2009).
- [26] H. Jaeger, *Tutorial on Training Recurrent Neural Networks, Covering BPPT, RTRL, EKF and the Echo State Network Approach* (GMD-Forschungszentrum Informationstechnik, Bonn, 2002), Vol. 5.
- [27] M. M. Waldrop, The chips are down for Moore's law, *Nature* **530**, 144 (2016).
- [28] I. L. Markov, Limits on fundamental limits to computation, *Nature* **512**, 147 (2014).
- [29] G. Tanaka, T. Yamane, J. B. Héroux, R. Nakane, N. Kanazawa, S. Takeda, H. Numata, D. Nakano, and A. Hirose, Recent advances in physical reservoir computing: A review, *Neural Netw.* **115**, 100 (2019).
- [30] K. Nakajima, Physical reservoir computing—an introductory perspective, *Jpn. J. Appl. Phys.* **59**, 060501 (2020).
- [31] Z. Deng and Y. Zhang, Collective behavior of a small-world recurrent neural system with scale-free distribution, *IEEE Trans. Neural Netw.* **18**, 1364 (2007).
- [32] T. Nishikawa, A. E. Motter, Y.-C. Lai, and F. C. Hoppensteadt, Heterogeneity in Oscillator Networks: Are Smaller Worlds Easier to Synchronize?, *Phys. Rev. Lett.* **91**, 014101 (2003).
- [33] Y. Kawai, J. Park, and M. Asada, A small-world topology enhances the echo state property and signal propagation in reservoir computing, *Neural Netw.* **112**, 15 (2019).
- [34] S. K. Bose, J. B. Mallinson, E. Galli, S. Acharya, C. Minnai, P. Bones, and S. A. Brown, Neuromorphic behaviour in discontinuous metal films, *Nanoscale Horiz.* **7**, 437 (2021).
- [35] D. J. Watts and S. H. Strogatz, Collective dynamics of “small-world” networks, *Nature* **393**, 440 (1998).
- [36] S. Fostner, R. Brown, J. Carr, and S. A. Brown, Continuum percolation with tunneling, *Phys. Rev. B* **89**, 075402 (2014).
- [37] Y. Yang, B. Chen, and W. D. Lu, Memristive physically evolving networks enabling the emulation of heterosynaptic plasticity, *Adv. Mater.* **27**, 7720 (2015).
- [38] D. Stauffer and A. Aharony, *Introduction to Percolation Theory* (CRC Press, Boca Raton, 2018).
- [39] J. Schmelzer, S. A. Brown, A. Wurl, M. Hyslop, and R. J. Blaikie, Finite-Size Effects in the Conductivity of Cluster

- Assembled Nanostructures, *Phys. Rev. Lett.* **88**, 226802 (2002).
- [40] D. B. Strukov, G. S. Snider, D. R. Stewart, and R. S. Williams, The missing memristor found, *Nature* **453**, 80 (2008).
- [41] K. Krishnan, T. Tsuruoka, C. Mannequin, and M. Aono, Mechanism for conducting filament growth in self-assembled polymer thin films for redox-based atomic switches, *Adv. Mater.* **28**, 640 (2016).
- [42] H. Yang, Z. Wang, X. Guo, H. Su, K. Sun, D. Yang, W. Xiao, Q. Wang, and D. He, Controlled growth of fine multifilaments in polymer-based memristive devices via the conduction control, *ACS Appl. Mater. Interfaces* **12**, 34370 (2020).
- [43] W. Wang, M. Wang, E. Ambrosi, A. Bricalli, M. Laudato, Z. Sun, X. Chen, and D. Ielmini, Surface diffusion-limited lifetime of silver and copper nanofilaments in resistive switching devices, *Nat. Commun.* **10**, 81 (2019).
- [44] A. N. Burkitt, A review of the integrate-and-fire neuron model: I. Homogeneous synaptic input, *Biol. Cybern.* **95**, 1 (2006).
- [45] W. Gerstner, W. M. Kistler, R. Naud, and L. Paninski, *Neuronal Dynamics* (Cambridge University Press, Cambridge, 2014).
- [46] J. B. Mallinson, Z. Heywood, R. K. Daniels, M. D. Arnold, P. J. Bones, and S. A. Brown, Reservoir computing using networks of memristors: Effects of topology and heterogeneity, *Nanoscale* **15**, 9663 (2023).
- [47] F. Harary, *Graph Theory* (Addison-Wesley Publishing Co., Boca Raton, 1969).
- [48] S. F. Muldoon, E. W. Bridgeford, and D. S. Bassett, Small-world propensity and weighted brain networks, *Sci. Rep.* **6**, 22057 (2016).
- [49] D. S. Bassett and E. T. Bullmore, Small-world brain networks revisited, *Neuroscientist* **23**, 499 (2017).
- [50] A. Loeffler, R. Zhu, J. Hochstetter, M. Li, K. Fu, A. Diaz-Alvarez, T. Nakayama, J. M. Shine, and Z. Kuncic, Topological properties of neuromorphic nanowire networks, *Front. Neurosci.* **14**, 184 (2020).
- [51] D. V. Foster, J. G. Foster, P. Grassberger, and M. Paczuski, Clustering drives assortativity and community structure in ensembles of networks, *Phys. Rev. E* **84**, 066117 (2011).
- [52] P. Holme and J. Zhao, Exploring the assortativity-clustering space of a network's degree sequence, *Phys. Rev. E* **75**, 046111 (2007).
- [53] S. Wasserman and K. Faust, *Social Network Analysis: Methods and Applications* (Cambridge university press, Cambridge, 1994).
- [54] M. E. Newman, Assortative Mixing in Networks, *Phys. Rev. Lett.* **89**, 208701 (2002).
- [55] B. Bentley, R. Branicky, C. L. Barnes, Y. L. Chew, E. Yemini, E. T. Bullmore, P. E. V ertes, and W. R. Schafer, The multilayer connectome of *Caenorhabditis elegans*, *PLoS Comput. Biol.* **12**, e1005283 (2016).
- [56] C. Blasche, S. Means, and C. R. Laing, Degree assortativity in networks of spiking neurons, *J. Comput. Dyn.* **7**, 401 (2020).
- [57] M. Roy, S. Poria, and C. Hens, Assortativity-induced explosive synchronization in a complex neuronal network, *Phys. Rev. E* **103**, 062307 (2021).
- [58] M. Rubinov and O. Sporns, Complex network measures of brain connectivity: Uses and interpretations, *J. Comput. Dyn.* **52**, 1059 (2010).
- [59] S. de Franciscis, S. Johnson, and J. Torres, Enhancing neural-network performance via assortativity, *Phys. Rev. E* **83**, 036114 (2011).